Title
Discovery of β-LnNiSb3 (Ln = La, Ce): Crystal Growth, Structure, and Magnetic and Transport Behavior

Journal
Inorganic Chemistry, 46(8)

ISSN
0020-1669

Authors
Thomas, Evan Lyle
Gautreaux, Dixie P
Lee, Han-Oh
et al.

Publication Date
2007-04-01

DOI
10.1021/ic0615832

Inorg. Chem. **2007**, *46*, 3010–3016

Discovery of β-$LnNiSb_3$ (Ln = La, Ce): Crystal Growth, Structure, and Magnetic and Transport Behavior

Evan Lyle Thomas,[†] Dixie P. Gautreaux,[†] Han-Oh Lee,[‡] Zachary Fisk,[§] and Julia Y. Chan*[,†]

Department of Chemistry, Louisiana State University, 232 Choppin Hall, Baton Rouge, Louisiana 70803, Department of Physics, University of California, One Shields Avenue, Davis, California 95616, and Department of Physics & Astronomy, University of California, 4129 Frederick Reines Hall, Irvine, California 92697

Received August 21, 2006

A new polymorph of $CeNiSb_3$ has been grown from a Sn flux and characterized by single-crystal X-ray diffraction. β-$CeNiSb_3$ crystallizes in the orthorhombic space group *Pbcm* (No. 57) with $Z = 8$. The unit cell parameters are $a = 12.9170(2)$ Å, $b = 6.1210(5)$ Å, $c = 12.0930(6)$ Å, and $V = 956.13(9)$ Å^3. Its layered structure contains structural motifs similar to that of the first form of $CeNiSb_3$ and consists of Ce atoms inserted between anionic layers of nearly square $_\infty^2$[Sb] nets and distorted $_\infty^2$[$NiSb_2$] octahedra. We report the synthesis, magnetization, electrical resistivity, and specific heat of the new form of $CeNiSb_3$ and compare the structures and physical properties of both polymorphs.

Introduction

Rare-earth intermetallics—particularly those consisting of a lanthanide (Ln), transition metal (T), and antimony—display interesting physical property behavior and also unique bonding within their structures.[1−3] The layered $LnTSb_3$ family, where T = V, Cr, Ni, and Pd, is studied because of the influence of the transition metals on both the anisotropic magnetic behavior and the crystal chemistry of these compounds. $LaCrSb_3$ ($a = 13.276(2)$, $b = 6.209(1)$, $c = 6.114(1)$ Å, $Z = 4$) orders ferromagnetically ($T_C \sim 125-146$ K)[4−7] as a result of the ordering of the Cr ions. More recent susceptibility data for single crystals of $LaCrSb_3$ show a coexistence of the ferromagnetic (FM) and antiferromagnetic (AFM) states below $T_C \sim 132$ K.[8−11] Susceptibility data for the Ce, Pr, Nd, and Sm analogues also show two magnetic transitions (FM at $T \sim 100-120$ K and AFM at $T < 30$ K).[4−6,12,13] The Gd analogue shows a ferrimagnetic transition at $T_C \sim 90$ K,[14,15] while the Tb and Dy analogues display only AFM ordering at temperatures below 17 K.[5] It is has been suggested that lanthanide contraction leads to the shift from FM to AFM ordering, which is favorable for rare-earth atoms.[5] However, $YbCrSb_3$ (Yb^{2+}) is reported to have the highest ordering temperature of any member of this series with $T_C \sim 280$ K.[16]

Substitution of Cr with Ni has led to the discovery of $CeNiSb_3$ [$a = 12.6340(7)$, $b = 6.2037(3)$, $c = 18.3698(9)$ Å, $Z = 12$] which displays Kondo lattice behavior and FM ordering below $T_C = 6$ K.[17,18] The $CeNiSb_3$ structure type is known to exist only when Ln = Pr, Nd, and Sm.[19] Each of

* To whom correspondence should be addressed. E-mail: jchan@lsu.edu. Phone: 225-578-2695. Fax: 225-578-3458.
[†] Louisiana State University.
[‡] University of California at Davis.
[§] University of California at Irvine.

(1) Mills, A. M.; Lam, R.; Ferguson, M. J.; Deakin, L.; Mar, A. *Coord. Chem. Rev.* **2002**, *233*, 207−222.
(2) Papoian, G. A.; Hoffmann, R. *Angew. Chem., Int. Ed.* **2000**, *39*, 2409−2448.
(3) *Rare Earth-Antimony Systems*; Sologub, O., Salamakha, P. S., Eds.; Elsevier: Amsterdam, 2003; Vol. 33.
(4) Hartjes, K.; Jeitschko, W.; Brylak, M. *J. Magn. Magn. Mater.* **1997**, *173*, 109−116.
(5) Leonard, M.; Saha, S.; Ali, N. *J. Appl. Phys.* **1999**, *85*, 4759−4761.
(6) Leonard, M. L.; Dubenko, I. S.; Ali, N. *J. Alloys Compd.* **2000**, *303*, 265−269.
(7) Raju, N. P.; Greedan, J. E.; Ferguson, M. J.; Mar, A. *Chem. Mater.* **1998**, *10*, 3630−3635.
(8) Granado, E.; Martinho, H.; Sercheli, M. S.; Pagliuso, P. G.; Jackson, D. D.; Torelli, M.; Lynn, J. W.; Rettori, C.; Fisk, Z.; Oseroff, S. B. *Phys. Rev. Lett.* **2002**, *89*, 107204.
(9) Jackson, D. D.; Torelli, M.; Fisk, Z. *Phys. Rev. B* **2002**, *65*, 014421.
(10) Richter, M.; Rusz, J.; Rosner, H.; Koepernik, K.; Opahle, I.; Nitzche, U.; Eschrig, H. *J. Mag. Magn. Mater.* **2004**, *272−276*, e251−e252.
(11) Shim, J. H.; Min, B. I. *J. Mag. Magn. Mater.* **2004**, *272−276*, e241−e242.
(12) Deakin, L.; Ferguson, M. J.; Mar, A.; Greedan, J. E.; Wills, A. S. *Chem. Mater.* **2001**, *13*, 1407−1412.
(13) Jackson, D. D.; Fisk, Z. *J. Magn. Magn. Mater.* **2003**, *256*, 106−116.
(14) Deakin, L.; Mar, A. *Chem. Mater.* **2003**, *15*, 3343−3346.
(15) Jackson, D. D.; Fisk, Z. *J. Alloys Compd.* **2004**, *377*, 243−247.
(16) Crerar, S. J.; Deakin, L.; Mar, A. *Chem. Mater.* **2005**, *17*, 2780−2784.

10.1021/ic0615832 CCC: $37.00
Published on Web 03/20/2007

these metallic, highly anisotropic compounds orders antiferromagnetically below 5 K.[19] Incidentally, further substitution of the transition metal with Pd has led to another structure, with $a = 12.780$, $b = 6.330$, $c = 12.453$ Å, and $Z = 8$.[20,21] Similar to $CeNiSb_3$, $CePdSb_3$ also exhibits Kondo lattice behavior; however, antiferromagnetism appears below $T_N \sim 3$ K.[20]

In our search for strongly correlated electronic systems,[22] we typically employ a metal(lic) flux-growth method as a synthetic route to obtaining single crystals of these materials. This technique has facilitated the characterization and study of several novel intermetallic phases. Our crystal growth experiments of $CeTSb_3$ (T = Ni, Pd), show that sample preparative conditions can influence the structural arrangements and thus the physical properties of these compounds. From the efforts to grow larger crystals of $CeNiSb_3$ for magnetic and transport measurements by using Sn rather than Sb as flux, we have discovered a new polymorph of this phase. The two polymorphs are similar with regards to their structures (containing Ce-capped $_\infty^2$[Sb] nets and $_\infty^2$[$NiSb_2$] octahedra with comparable distortions) and their physical properties (Kondo lattice behavior, large magnetic anisotropy, and enhanced C/T at their magnetic transitions).

In this paper, we describe the synthesis of the new form of $CeNiSb_3$ (hereafter β-$CeNiSb_3$) and compare the structures of the two polymorphs along with a relationship to the $CeCrSb_3$-type structure. Furthermore, magnetization, electrical resistivity, and specific heat data are also presented and compared.

Experimental Section

Synthesis. Single crystals of β-$LaNiSb_3$ and β-$CeNiSb_3$ were grown via a flux-growth method using excess Sn. La and Ce ingot (99.9%), Ni powder (99.999%), Sb shot (99.999%), and Sn shot (99.8%) were purchased from Alfa Aesar and weighed and then combined into a 5 mL alumina crucible in a 1:1:3:20 (Ln:Ni:Sb:Sn) molar ratio. (Tin was chosen as a flux because of its lower melting point compared to that of Sb, which would allow for a longer cooling window and the formation of larger single crystals.) The crucible was then covered with quartz wool and sealed into an evacuated fused-silica tube. The reaction vessel was heated to a temperature of 1423 K and held constant for 8 h and then cooled at a rate of 5 K h^{-1} to 523 K (just above the melting point of Sn metal). After the temperature reached 523 K, the excess Sn was separated from the single crystals by centrifugation. Thin and brittle, shiny, black, sheetlike crystals with dimensions up to $0.10 \times 3 \times 5$ mm^3 were mechanically extracted from the product. Crystals with topical flux were etched in concentrated HCl for several minutes. There were no signs of surface oxidation when the crystals were exposed to air and moisture over a period of weeks.

Table 1. Crystallographic Data for β-$LnNiSb_3$ (Ln = La, Ce)

	$LaNiSb_3$	$CeNiSb_3$
formula units (amu)	562.87	564.08
space group	*Pbcm*	*Pbcm*
cryst system	orthorhombic	orthorhombic
a (Å)	13.0970(2)	12.9170(2)
b (Å)	6.1400(4)	6.1210(5)
c (Å)	12.1270(4)	12.0930(6)
V (Å^3)	975.20(7)	956.13(9)
Z	8	8
dimens min/mid/max (mm^3)	0.050/0.050/0.10	0.080/0.080/0.10
temp (K)	298(2)	298(2)
calcd density (g cm^{-3})	7.668	7.837
θ range (deg)	1.55−30.03	3.15 - 29.99
μ (mm^{-1})	28.573	29.728
T_{min}/T_{max}	0.1749/0.2396	0.0739/0.0927
collected reflcns	2677	2601
independent reflcns	1491	1445
R_{int}	*0.0396*	*0.0181*
h	$-18 \le h \le 18$	$-17 \le h \le 18$
k	$-8 \le k \le 8$	$-8 \le k \le 8$
l	$-16 \le l \le 16$	$-16 \le l \le 16$
data/params/restraints	1491/53/0	1445/53/0
goodness of fit on F_o^2	1.110	1.118
$\Delta\rho_{max}$ (e Å^{-3})	7.528	5.514
$\Delta\rho_{min}$ (e Å^{-3})	−5.625	−1.705
extinction coeff	0.0056(5)	0.00030(7)
$R_1(F)$ for $F_o^2 > 2\sigma(F_o^2)$[a]	0.0627	0.0282
$R_w(F_o^2)$[b]	0.1779	0.0716

[a] $R_1(F) = \sum||F_o| - |F_c||/\sum|F_o|$. [b] $R_w(F_o^2) = \sum[w(F_o^2 - F_c^2)]/\sum[w(F_o^2)^2]^{1/2}$; $w = 1/[\sigma^2(F_o^2) + (0.1403P)^2 + 1.2064P]$ and $w = 1/[\sigma^2(F_o^2) + (0.0140P)^2 + 12.8728P]$, where $P = (F_o^2 + 2F_c^2)/3$ for Ln = La and Ce, respectively.

Single crystals from the β-$LnNiSb_3$ (Ln = La, Ce) samples were ground into a fine powder, placed on a no-background holder, and screened for homogeneity and possible impurity phases using powder X-ray diffraction on a Bruker D-8 X-ray diffractometer with monochromatized Cu Kα radiation, $\lambda = 1.540562$ Å. Sample homogeneity was also confirmed by conducting lattice determinations on several crystals using single-crystal X-ray diffraction. The experimental powder pattern was compared to the calculated powder pattern generated from the refined structure of β-$CeNiSb_3$.

Single-Crystal X-ray Diffraction. A mechanically fragmented, block-shaped crystal of β-$CeNiSb_3$ with dimensions of $\sim 0.080 \times 0.080 \times 0.10$ mm^3 was mounted onto the tip of the glass fiber of a goniometer with epoxy and placed on a Nonius Kappa CCD X-ray diffractometer (Mo Kα radiation, $\lambda = 0.710\,73$ Å). Room-temperature data collection parameters and other crystallographic data are listed in Table 1. The orthorhombic Laue symmetry *mmm* and systematic absences found led to the selection of space group *Pbcm* (No. 57), transformed from the nonstandard setting *Pbma*. The initial structural model was generated using SIR97[23] and then refined using the SHELXL97 package.[24] Refinement of the atomic positions led to a further correction of the data by the calculation of an extinction coefficient and also by the anisotropic refinement of the displacement parameters. As a check for deviations from the ideal stoichiometry, the atomic occupancy parameters were refined in separate sets of least-squares cycles. Since no considerable deviations were observed, each atomic site in β-$CeNiSb_3$ may be considered fully occupied. [Partial occupancies were observed on

(17) Macaluso, R. T.; Wells, D. M.; Sykora, R. E.; Albrecht-Schmitt, T. E.; Mar, A.; Nakatsuji, S.; Lee, H.; Fisk, Z.; Chan, J. Y. *J. Solid State Chem.* **2004**, *177*, 293−298.
(18) Sidorov, V. A.; Bauer, E. D.; Lee, H.; Nakatsuji, S.; Thompson, J. D.; Fisk, Z. *Phys. Rev. B* **2005**, *71*, 094422.
(19) Thomas, E. L.; Macaluso, R. T.; Lee, H.-O.; Fisk, Z.; Chan, J. Y. *J. Solid State Chem.* **2004**, *177*, 4228−4236.
(20) Thamizhavel, A.; Nakashima, H.; Shiromoto, T.; Obiraki, Y.; Matsuda, T. D.; Haga, Y.; Ramakrishnan, S.; Takeuchi, T.; Settai, R.; Ōnuki, Y. *J. Phys. Soc. Jpn.* **2005**, *74*, 2617−2621.
(21) Thomas, E. L.; Gautreaux, D. P.; Chan, J. Y. *Acta Crystallogr., Sect. E: Struct. Rep. Online* **2006**, *62*, I96−I98.
(22) Thomas, E. L.; Millican, J. N.; Okudzeto, E.; Chan, J. Y. *Comments Inorg. Chem.* **2006**, *27*, 1−39.
(23) Altomare, A.; Burla, M. C.; Camalli, M.; Cascarno, G. L.; Giacovazzo, A.; Guagliardi, A.; Moliterni, A. G. G.; Polidori, G.; Spagna, R. *J. Appl. Crystallogr.* **1999**, *32*, 115−119.
(24) Sheldrick, G. M. In *SHELXL-97, Program for Refinement of Crystal Structures*; University of Göttingen: Göttingen, Germany, 1997.

Table 2. Atomic Positions, Wyckoff Site Symmetry, and U_{eq} Values for β-LnNiSb$_3$ (Ln = La, Ce)

atom	Wyckoff site	*x*	*y*	*z*	U_{eq} (Å^2)[a]
La1	4*c*	0.69985(7)	$^1/_4$	0	0.0077(3)
La2	4*d*	0.30410(7)	0.26099(11)	3/4	0.0077(3)
Ni1	8*e*	0.10248(10)	0.0302(2)	0.86359(9)	0.0105(4)
Sb1	4*c*	0.97547(8)	$^1/_4$	0	0.0128(3)
Sb2	4*d*	0.78994(8)	0.25128(12)	3/4	0.0080(3)
Sb3	8*e*	0.50131(5)	0.50751(9)	0.87603(4)	0.0087(3)
Sb4	4*c*	0.21479(8)	$^1/_4$	0	0.0079(3)
Sb5	4*d*	0.94673(7)	0.88313(14)	3/4	0.0121(3)
Ce1	4*c*	0.69921(4)	$^1/_4$	0	0.00697(13)
Ce2	4*d*	0.30482(4)	0.26209(7)	3/4	0.00675(13)
Ni1	8*e*	0.10429(6)	0.03016(13)	0.86352(6)	0.00943(18)
Sb1	4*c*	0.97482(5)	$^1/_4$	0	0.01116(15)
Sb2	4*d*	0.78593(5)	0.25134(8)	3/4	0.00747(15)
Sb3	8*e*	0.50154(3)	0.50804(6)	0.87596(3)	0.00812(13)
Sb4	4*c*	0.21859(5)	$^1/_4$	0	0.00734(15)
Sb5	4*d*	0.94614(4)	0.88374(10)	3/4	0.01086(15)

[a] U_{eq} is defined as one-third of the trace of the orthogonalized $\mathbf{U}_{ij}$ tensor.

Table 3. Selected Interatomic Distances (Å) in β-CeNiSb$_3$

Ce1−Sb1	3.5601(8)	Ni1−Ni1	2.7456(15)
Ce1−Sb2 (×2)	3.2241(3)	Ni1−Sb1	2.5901(8)
Ce1−Sb3 (×2)	3.3419(5)	Ni1−Sb1	2.7076(9)
Ce1−Sb3 (×2)	3.3562(5)	Ni1−Sb2	2.6093(9)
Ce1−Sb4 (×2)	3.2395(3)	Ni1−Sb4	2.5913(8)
		Ni1−Sb5	2.6193(9)
Ce2−Ni1	3.2572(9)	Ni1−Sb5	2.6444(10)
		Sb1−Sb1	3.1289(4)
Ce2−Sb2	3.2159(7)	Sb1−Sb4	3.1488(9)
Ce2−Sb2	3.3388(7)	Sb1−Sb5	3.2943(3)
Ce2−Sb3 (×2)	3.3158(6)	Sb2−Sb5	3.0571(8)
Ce2−Sb3 (×2)	3.3232(6)	Sb3−Sb3	3.0020(7)
Ce2−Sb4 (×2)	3.2227(3)	Sb3−Sb3	3.0464(7)
Ce2−Sb5	3.3261(7)	Sb3−Sb3	3.0607(6)

the T (4*c*) and Sb1 (4*d*) sites of CeTSb$_3$ (T = V, Cr).[25]] In the final refinement procedure of β-CeNiSb$_3$, a weighting scheme was calculated which gave $R_1 = 0.0282$ and $R_w = 0.0716$. The highest peak and deepest hole in the electron density map were 5.514 and −1.705 e Å^{-3}, which are 0.91 and 0.65 Å, respectively, from Sb5. Atomic coordinates and anisotropic displacement parameters are given in Table 2, and selected interatomic distances are listed in Table 3. Detailed information on the data collections in CIF format is provided as Supporting Information.

Physical Properties. Magnetic measurements on single crystals were performed using a Quantum Design Magnetic Property Measurement System (MPMS) superconducting quantum interference device (SQUID) magnetometer. Zero-field-cooled (ZFC) temperature-dependent susceptibility data were measured with an applied field of 0.1 T from 1.8 to 330 K, and then field-cooled (FC) measurements were taken by cooling the sample from room temperature to 1.8 K. The field-dependent susceptibility was measured up to 7 T at 2 K. The resistivity data were measured using a standard four-probe method down to 1.8 K with a Quantum Design Physical Property Measurement System (PPMS) at ambient pressure. The specific heat was measured with a Quantum Design PPMS using a thermal relaxation method from 0.4 to 20 K in zero applied field. The entropy data was calculated by integrating the specific heat divided by the temperature.

Results and Discussion

Structure. The ternary antimonides CeTSb$_3$ (T = V, Cr, Ni, Pd) all crystallize in the *Pbcm* space group in one of three structure types: CeCrSb$_3$,[25] CeNiSb$_3$[26] or CePdSb$_3$.[20,21]

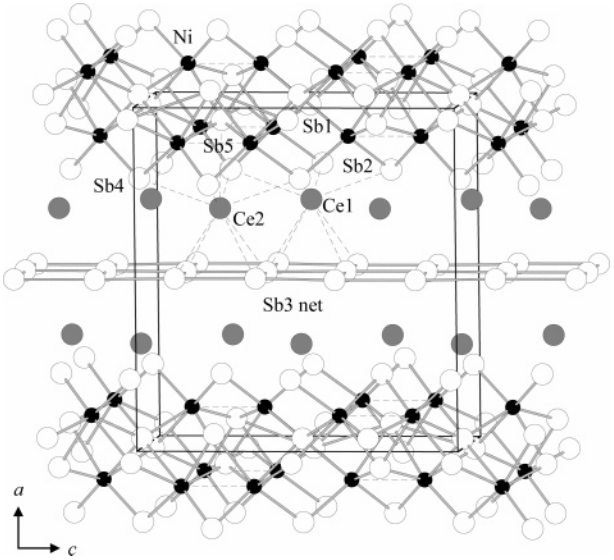

Figure 1. Crystal structure of β-CeNiSb$_3$ with the unit cell outlined. The shaded circles are Ce atoms, the solid circles are Ni atoms, and the open circles are Sb atoms. The bonding environments of Ce1 and Ce2 are shown as dashed lines. Ce2 adopts a monocapped square antiprismatic environment, while Ce1 adopts a square antiprismatic environment.

The V and Cr analogues are isostructural to CeCrSb$_3$ [a = 13.108(3), b = 6.184(1), c = 6.079(1) Å],[25] while the first reported Ni analogue (hereafter α-CeNiSb$_3$) has cell dimensions of a = 12.6340(7), b = 6.2037(3), and c = 18.3698(9) Å.[17] The Pd analogue[20] and the new form of the Ni analogue [a = 12.9170(2), b = 6.1210(5), c = 12.0930(6) Å] presented here are isomorphous. Each of these layered structures contain similar subunits, including two-dimensional square or nearly square Sb nets ($_\infty^2$[Sb]) capped by Ce^{3+} atoms and TSb$_6$ octahedra ($_\infty^2$[TSb$_2$]) stacked along the *a*-direction.

Figure 1 shows the ball and stick representation for β-CeNiSb$_3$. While both forms of CeNiSb$_3$ contain two crystallographically inequivalent Ce atoms, in the β-form these atoms have different coordinations. The Ce1 (4*c*) atoms

(25) Brylak, M.; Jeitschko, W. *Z. Naturforsch., B* **1995**, *50*, 899−904.

(26) Macaluso, R. T.; Sarrao, J. L.; Pagliuso, P. G.; Moreno, N. O.; Goodrich, R. G.; Browne, D. A.; Fronczek, F. R.; Chan, J. Y. *J. Solid State Chem.* **2002**, *166*, 245−250.

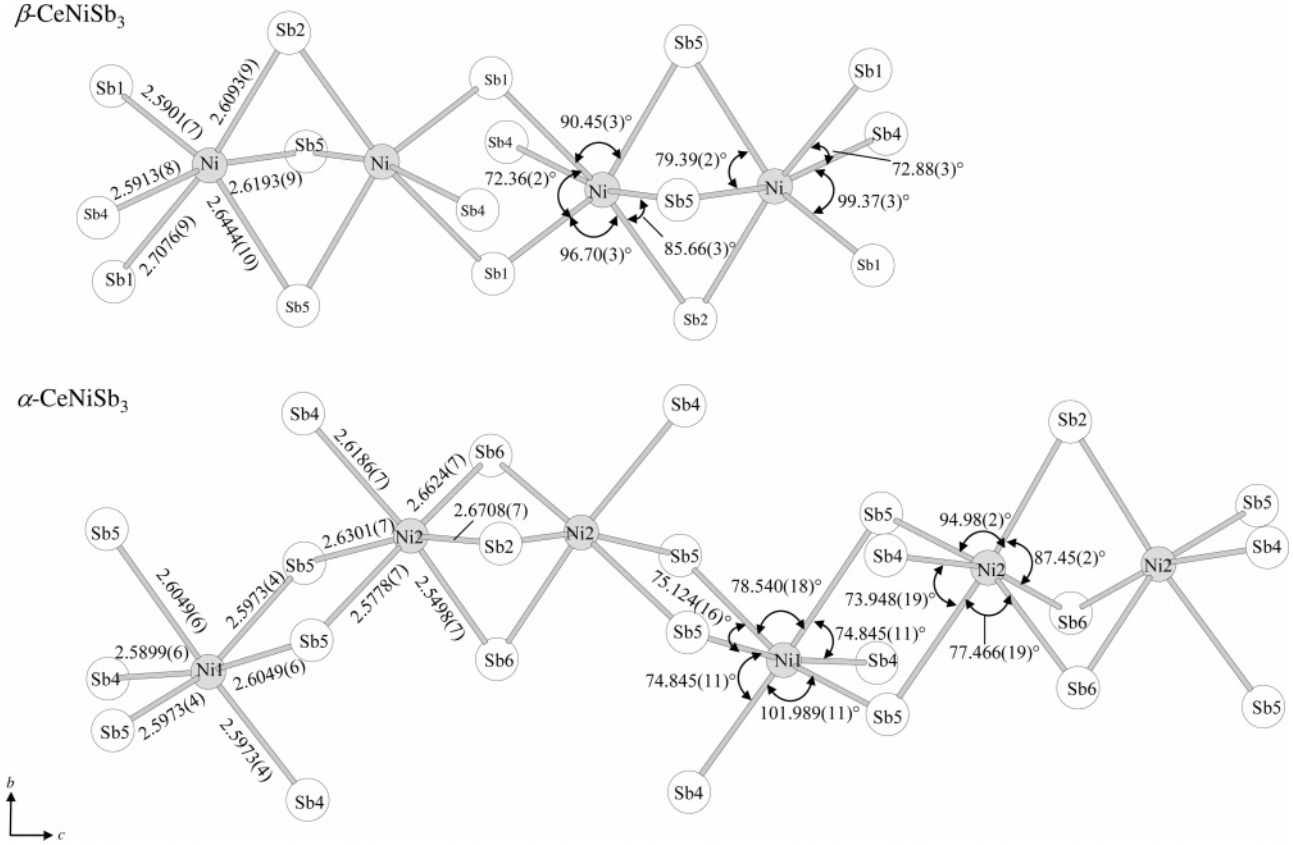

Figure 2. Projection of the $_{\infty}^{2}$[$NiSb_2$] polyhedra along the *bc*-plane of both $CeNiSb_3$ forms.

are surrounded by 8 Sb atoms adopting a square antiprismatic geometry where 4 Sb atoms of the Sb3 net form a square base and 4 Sb atoms from the $_{\infty}^{2}$[$NiSb_2$] layer form a slightly larger square directly above but twisted 45° in relation to the first square. On the other hand, the Ce2 (4*d*) atoms are surrounded by 9 Sb atoms and adopt a monocapped square antiprismatic geometry similar to the geometry of Ce1 but with an additional Sb5 atom capping the larger second square. It should be noted that there is also an Sb1 atom in the capping position of Ce1 at a distance of 3.5601(8) Å; however, we consider this distance too far for strong bonding. In α-$CeNiSb_3$, both Ce atoms have identical geometries with Ce1 (4*d*) being bonded to 4 Sb1, 2 Sb2, 2 Sb4, and 1 Sb6 atoms and Ce2 (8*e*) being bonded to 2 Sb1, 1 Sb2, 2 Sb3, 3 Sb4, and 1 Sb5 atoms.[17] The Ce atoms in both forms are staggered above and below the $_{\infty}^{2}$[Sb] nets. In *β*-$CeNiSb_3$, the Ce1−Sb distances of 3.2241(3)−3.3562(8) Å and the Ce2−Sb distances of 3.2159(7)−3.3388(7) Å are comparable to the Ce1−Sb distances of 3.2225(3)−3.3112(6) Å and Ce2−Sb distances of 3.2260(3)−3.4509(4) Å in α-$CeNiSb_3$.[17]

As shown in Figure 2, the $_{\infty}^{2}$[$NiSb_2$] octahedra of *β*-$CeNiSb_3$ connect in a manner different from that for the octahedra found within α-$CeNiSb_3$. These $_{\infty}^{2}$[$NiSb_2$] octahedra are edge-sharing in *b* and both edge- and face-sharing in *c* in both phases. The Ni−Sb bond distances in *β*-$CeNiSb_3$ range from 2.5901(8) to 2.7076(9) Å, which on average are slightly longer but comparable to the Ni−Sb distances in α-$CeNiSb_3$, which range from 2.5498(7) to 2.6708(7) Å,[17] and also to the Ni−Sb distances of 2.5675 Å in the $NiSb_6$ octahedra in NiSb (NiAs-type).[27] Angles between the Ni and Sb atoms in both forms diverge considerably from the ideal 90°. Furthermore, the Ni metal−metal interactions are present in both forms and occur at the adjourning octahedral faces with Ni−Ni distances of 2.7456(15) Å in the *β*-form and Ni2−Ni2 distances of 2.7214(12) Å in the α-form.[17]

The major distinction with $CeCrSb_3$, α-$CeNiSb_3$, and *β*-$CeNiSb_3$ lies in the connectivity, or packing, of the TSb_6 octahedra along *c*. Figure 3a−c shows the polyhedral representations and relationship of these structures. It becomes obvious in this series of compounds that the structure type adopted is a function of the transition metal. The $NiSb_6$ octahedra in *β*-$CeNiSb_3$ (Figure 3b) are edge-sharing in the *b*-direction and both edge- and face-sharing in the *c*-direction, resulting in an approximate doubling of the *c*-parameter [$c = 12.0930(6)$ Å] when compared to that of $CeCrSb_3$ (Figure 3a). The $_{\infty}^{2}$[$NiSb_2$] octahedra in α-$CeNiSb_3$ (Figure 3c) are edge-sharing in *b* and edge- and face-sharing in *c*, however with two different types of edge-sharing octahedra in *c*.[17] This gives rise to an approximate tripling of its *c*-parameter [$c = 18.3698(9)$ Å] in comparison to $CeCrSb_3$. For reference, the $_{\infty}^{2}$[$CrSb_2$] octahedra are edge-sharing along *b* and only face-sharing along *c*.[25] Furthermore, we find that the $_{\infty}^{2}$[$NiSb_2$] octahedra in *β*-$CeNiSb_3$ are less distorted than the $_{\infty}^{2}$[$NiSb_2$] octahedra of α-$CeNiSb_3$ but more distorted than the $_{\infty}^{2}$[$CrSb_2$] octahedra of $CeCrSb_3$.

The infinite, nearly square $_{\infty}^{2}$[Sb] nets of both $CeNiSb_3$ forms are shown in Figure 4. In the *β*-form, Sb3 (8*e*) atoms

(27) Chen, T.; Mikkelsen, J. C.; Charlan, G. B. *J. Cryst. Growth* **1978**, *43*, 5−12.

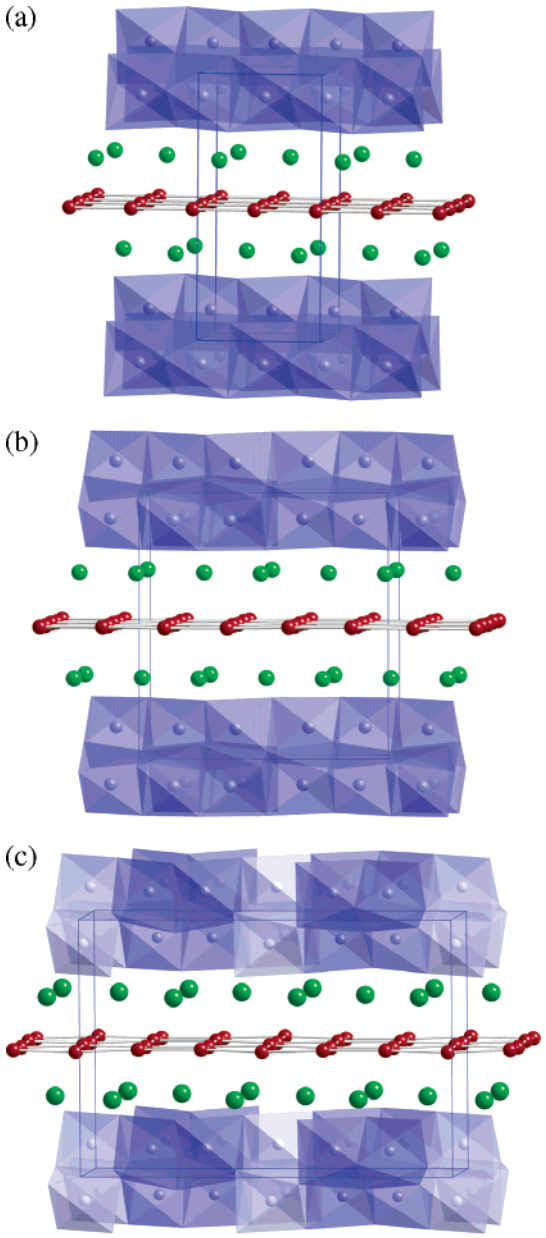

Figure 3. Polyhedral representations of the structures of (a) $CeCrSb_3$, (b) β-$CeNiSb_3$, and (c) α-$CeNiSb_3$ viewed in the *ac*-plane. The green circles are Ce atoms, and the maroon circles are Sb atoms. The blue-shaded octahedra represent TSb_6. The dark blue and light blue polyhedra distinguish the two inequivalent crystallographic Ni atom sites.

form these nets, while both Sb1 (8*e*) and Sb3 (4*c*) atoms bond to form the square nets in the α-form. Sb−Sb distances in the β-form range 3.0020(7)−3.0608(3) Å, shorter when compared to the Sb−Sb distances of 3.0616(3)−3.1035(2) Å in the α-form.[17] These distances are similar to the Sb−Sb distances of 2.908−3.355 Å in elemental antimony.[28] Yet still, the Sb−Sb bonds within the $_\infty^2$[Sb] nets in the α-form are more uniform. We note that the buckling of these nets in the α-form is more pronounced than in the β-form as shown in Figure 4, with Sb−Sb−Sb angles in the α-form ranging 84.95(1)−94.94(1)° [17] compared to angles of 88.113-(14)−91.868(14)° in the β-form.

Structural Stability. To determine the structural stability of β-$CeNiSb_3$, we performed several syntheses. β-$CeNiSb_3$ can only be obtained in high yield when samples are slowly cooled to just above the melting point of Sn (~505 K). From the reactions of Ce, Ni, and Sb in excess Sn, the yields of β-$CeNiSb_3$ are typically low, with the major impurity phase Ni_3Sn_4 and lesser amounts of Sn metal. We note that via an Sb flux-growth method, α-$CeNiSb_3$ is obtained when samples are removed from the furnace above the melting point of Sb (~943 K) to avoid Sb deposition on the crystal surfaces. Furthermore, use of the arc-melting technique followed by subsequent annealing using Ce, Ni, and Sb also led to homogeneous α-$CeNiSb_3$.

Experiments to transform α-$CeNiSb_3$ into β-$CeNiSb_3$ were also conducted. Single crystals (82.6 mg) of α-$CeNiSb_3$ were combined with 350 mg (or a 20-fold excess) of Sn shot and placed in an alumina crucible and covered with quartz wool. This sample was sealed under vacuum in a fused-silica tube and heated to 1423 K where it remained for 24 h and then cooled at 5 K h^{-1} to 573 K. Upon reaching 573 K, the molten Sn was removed by centrifugation. Although the reaction was heated for only 24 h and cooled for ~7 days, a noticeable amount of the α-form was converted into the β-form as confirmed by subsequent X-ray diffraction data collections. Other phases present in the powder diffraction patterns from the above reaction were exclusively unconverted α-$CeNiSb_3$ and Sn. These experiments suggest that β-$CeNiSb_3$ is a metastable phase in which there is no Sn present within the structure and that α-$CeNiSb_3$ may be dissolved by Sn, which plays an important role in the reduction of the activation energy barrier necessary to convert the α-from to the β-form.

While we can stabilize the β polymorph when samples are removed from the furnace at 523−573 K, we note that the β polymorph can also be stabilized at higher temperatures such as when samples are spun at 943 and 723 K. However, the yield is typically low when samples are removed at higher temperatures, compared to when samples are removed at 573 K. This suggests that the stability of β-$LnNiSb_3$ (Ln = La, Ce) is kinetically rather than thermodynamically driven. In addition, we have attempted several syntheses using other flux metals such as In (mp = 430 K) and Bi (mp = 544 K). However, β-$LnNiSb_3$ (Ln = La, Ce) can only be synthesized using Sn flux under our growth conditions.

Physical Properties. β-$CeNiSb_3$ single crystals have a rectangular thin platelike morphology with the out-of-the-plate axis as the crystalline *a*-axis. In the plane, however, we have not distinguished the *b*- and *c*-axes. From a comparison of the magnetic property data with those of the α-phase, we assume the ferromagnetic easy axis is the *c*-axis. The temperature-dependent magnetic susceptibility [$\chi(T)$] in an applied field of 0.1 T between 1.8 and 30 K for a single, plate-shaped crystal of β-$CeNiSb_3$ (1.99 mg) is shown in Figure 5. A spontaneous magnetic moment develops below 6 K with the applied magnetic field along *c*-axis, similar to what is observed in the $\chi(T)$ of the α-form.[29] A weaker

(28) Donohue, J. *The Structures of the Elements*; John Wiley & Sons: New York, 1974.

(29) Lee, H.-O.; Nakatsuji, S.; Chen, Y.; Bao, W.; Hundley, M. F.; Macaluso, R. T.; Chan, J. Y.; Carter, B.; Klavins, P.; Schlottmann, P.; Fisk, Z. Unpublished.

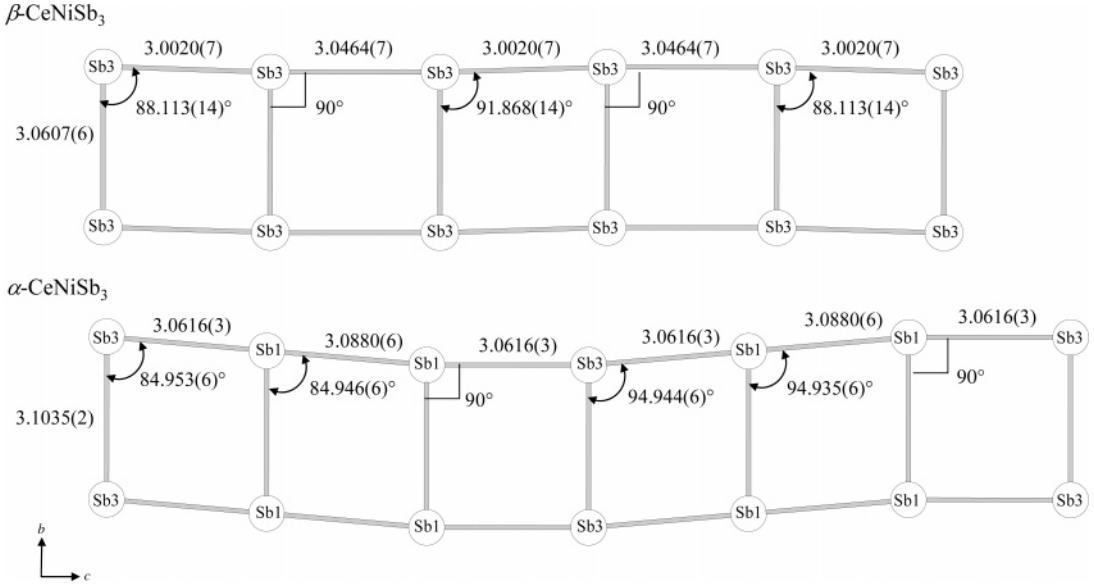

Figure 4. $_{\infty}^{2}$[Sb] square nets in β-$CeNiSb_3$ and α-$CeNiSb_3$[17] with bond distances in Å.

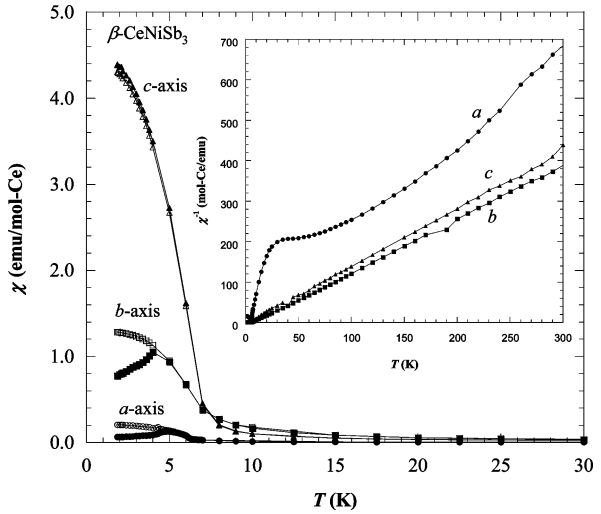

Figure 5. Anisotropic data from ZFC (closed markers) and FC (open markers) measurements of the temperature dependence (T) of the magnetic susceptibility (χ) for a single crystal of β-$CeNiSb_3$ ($H = 0.1$ T). Inset: ZFC inverse magnetic susceptibility data. Lines are drawn to guide the eye.

ferromagnetic (FM) feature appears along the *a*- and *b*-axes. Differences (anisotropy) between the ZFC and FC measurements along the crystallographic *a*- and *b*-axes may be due to the FM character of the spins along these directions as well as along the *c*-axis. The most distinct difference in the susceptibility data of α-$CeNiSb_3$ and β-$CeNiSb_3$ occurs when $H \parallel b$. In the β-form, there is a FM character of the *b*-axis, whereas in α-phase the susceptibility shows antiferromagnetic (AFM) behavior along this direction.[29] The inverse susceptibility (χ^{-1}) for β-$CeNiSb_3$ is shown in the inset of Figure 5. The χ along each direction obeys Curie−Weiss law [$\chi = C/(T - \theta)$] at high temperatures (above 100 K) with effective moments of 1.80, 2.54, and 2.38 μ_B and Weiss temperatures (θ) of 22.8, 8.4, and 1.4 K when oriented along the *a*−*c*-axes, respectively, with average μ_{eff} of 2.26 μ_B, slightly less than the calculated 2.54 μ_B for the Ce^{3+} free ion. The effective moments obtained from fits to the χ^{-1} data for the α-phase are 2.93, 2.39, and 2.37 μ_B, with θ values of −156, −2.3, and 29 K with the applied magnetic fields along the crystalline *a*−*c*-axes, respectively.[29] An average 2.58 μ_B/Ce is obtained, which is closer to the expected value for Ce^{3+}.[29] In the β-phase, the large positive θ value along the *a*-axis may be attributed to the strong interactions between atoms surrounding Ce in the crystal lattice in addition to the magnetic fluctuation of the *f*-moments. Yet, in contrast to the α-phase, where the θ values are negative along the *a*- and *b*-axes and positive along the *c*-axis, the Weiss temperatures are positive in the β-phase, which suggests the existence of FM components along all three directions and is consistent with the FM susceptibility at low temperatures along the *b*-axis.

The magnetization as a function of field, $M(H)$, for β-$CeNiSb_3$ at 2 K is shown in Figure 6. The magnetization saturates quickly along the *c*-axis with a saturation moment of ∼1.2 μ_B/Ce, indicating this axis as an easy axis. Along the *b*-axis, saturation begins to appear above 1 T and reaches a saturation moment of ∼1.6 μ_B/Ce, while, along the *a*-axis, a saturation moment of ∼0.35 μ_B/Ce is reached above ∼5 T. The magnetic moments obtained along each direction are slightly smaller than the theoretical saturation moment ($\mu_{sat} = gJ$) of 2.14 μ_B/Ce. The saturation moments of α-$CeNiSb_3$ are 0.5, 1.04, and 1.55 (easy axis) μ_B/Ce along the *a*−*c*-axes, respectively.[29] Interestingly, the magnitude of the saturation moments along *b*- and *c*-axes in the β-phase differs from the α-phase. While the largest moment is along the easy *c*-axis in the α-phase, the largest moment appears along the *b*-axis instead of the FM easy *c*-axis in the β-phase. α-$CeNiSb_3$ has a FM spin spiral structure with strong FM behavior along the *c*-axis, weak FM behavior along the *a*-axis, and AFM behavior along the *b*-axis.[29] In β-$CeNiSb_3$ however, all three axes show FM behavior, implying that the FM spins do not remain in the *ac*-plane, but there is an

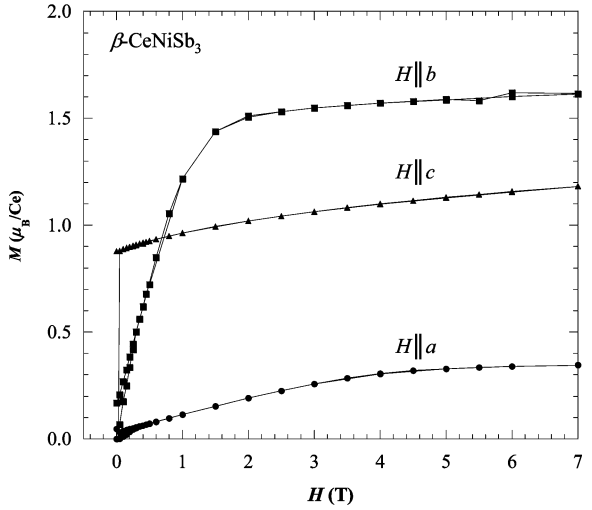

Figure 6. Field dependence of the magnetization, $M(H)$, at 2 K for a single crystal of β-$CeNiSb_3$.

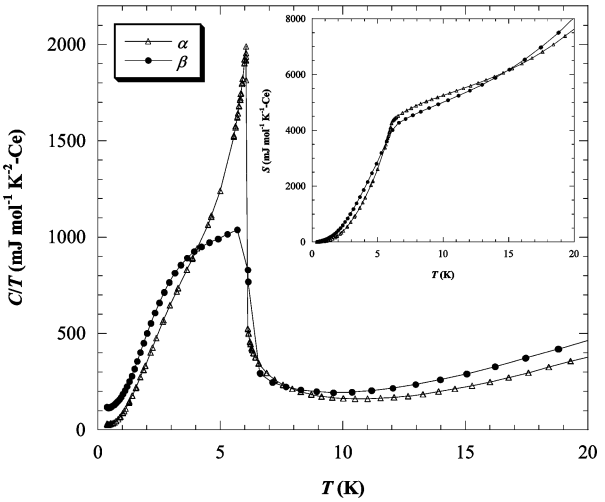

Figure 7. Specific heat and entropy in zero field for α-$CeNiSb_3$[17] (open triangles) and β-$CeNiSb_3$ (closed circles).

FM component along the *b*-axis as well. It is worthwhile to note that the Sb nets in the *bc*-plane (as shown in Figure 4) are more distorted in the α-phase. It is not clear whether the spiral type spin arrangement is present in β-$CeNiSb_3$. The different geometries of the Ce1 and Ce2 atoms in the β-phase may cause two different types of spin alignments along the Ce1−Ce2 nets which may cause a more complicated magnetic structure and affect the magnitude of the saturation moment. This could also be responsible for the FM behavior observed along the *b*-axis.

Specific heat (C/T) data for α-$CeNiSb_3$ and β-$CeNiSb_3$ are shown in Figure 7. A single peak is observed at $T \sim 6$ K for both compounds. This transition is very sharp for the α-phase and broader for the β-phase, which corresponds to the transition to FM ordering at the same temperature in the susceptibility data and also to the drops in the electrical resistivity data. The broad peak in the β-phase could be related to the sample quality. However, if this behavior is intrinsic, a different spin wave of the *f*-moment from the α-phase may be responsible. The γ value estimated from the fitting to $C/T = \gamma + AT^2$ is ∼60 mJ/(mol K^2), showing a moderate Kondo effect similar to that for α-$CeNiSb_3$.[18]

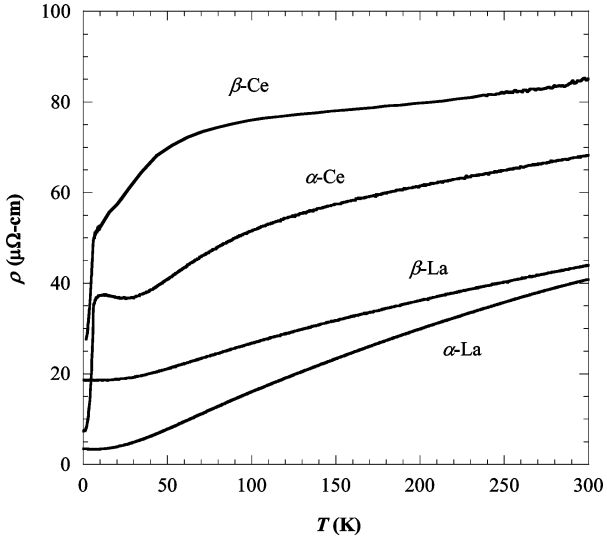

Figure 8. Temperature dependence of the electrical resistivity, $\rho(T)$, measured along the *bc*-plane for single crystals of the La and Ce analogues of both $CeNiSb_3$ forms.

The entropy at the transition temperature is ∼4100 mJ/(mol of Ce K), which is around 70% of R ln 2, where R (∼8314 mJ/(mol K)) is a gas constant. Assuming the ground state before the FM transition has a doubly degenerate spin-state, R ln 2 of entropy is expected at the transition temperature if there is no Kondo effect. The reduced entropy at T_C here, therefore, suggests the existence of the Kondo effect, similar to that for α-$CeNiSb_3$.[18]

The temperature dependence of the electrical resistivity, $\rho(T)$, for single crystals of α- and β-$LnNiSb_3$ (Ln = La, Ce) measured along the *b*-axis is shown in Figure 8. The transport data for α-$CeNiSb_3$ have been reported previously.[17] Metallic, Kondo lattice behavior is observed in β-$CeNiSb_3$, while the La analogues of both phases show simple metallic behavior. A broad shoulder appears at high temperatures for α- and β-$CeNiSb_3$ and suddenly drops at 6 K which coincides with the transition to FM order in the χ data. The broad peak feature around 100 K in the $\rho(T)$ of the α-phase is shifted to ∼70 K in the β-phase and may be attributed to the change in the crystalline electric field of neighboring atoms to Ce in the crystal lattice. Upon subtraction of the $\rho(T)$ of the β-La compound, a logarithmic temperature dependence of the resistivity at high temperatures is observed. This is suggestive of a typical Kondo lattice with a FM ground state and a moderate Kondo effect similar to that for α-$CeNiSb_3$.

Acknowledgment. We thank Peter Klavins of the Department of Physics at the University of California, Davis, CA. J.Y.C. acknowledges an NSF-CAREER award (Grant DMR 0237664) and Alfred P. Sloan Fellowship for partial support of this project. Z.F. acknowledges Grant DMR-NSF 0433560 for partial support of this project.

Supporting Information Available: X-ray crystallographic data in CIF format. This information is available free of charge via the Internet at http://pubs.acs.org.

IC0615832